International Journal on Advanced Science Engineering Information Technology

Vol.10 (2020) No. 3
ISSN: 2088-5334

Modeling and Simulation of a DC Micro-Grid with a Model Predictive Controller

Vladimir Prada[a,1], Oscar I. Caldas[a,2], Edilberto Mejía-Ruda[a,3], Mauricio Mauledoux[a,4], Oscar F. Avilés[a,5]

[a] *Davinci Research Group, Universidad Militar Nueva Granada, Bogotá, Colombia*
E-mail: [1]vladmont@gmail.com; [2]oscar.caldas@unimilitar.edu.co; [3]edilberto.mejia@unimilitar.edu.co; [4]mauricio.mauledoux@unimilitar.edu.co; [5]oscar.aviles@unimilitar.edu.co

***Abstract*— This paper presents the modeling strategies of a micro-grid to control the power supply of a battery bank by adopting a Model Predictive Controller (MPC). The grid was sized to light two tennis courts at a university sports complex, which is not connected to the national power grid and thus must be a stand-alone setup. The paper starts with an introduction that defines the statement of purpose and the state of the art. Then continue with the power generators and storage modeling: photovoltaic (PV) modules, wind turbine, buck converter (takes power from the rectified national grid) and the battery bank. The MPC was designed to effectively manage the energy supplied to the batteries, depending on the state of charge, hence the controller output is the signal used to regulate the charging current. The data used for prediction is the meteorological measures taken during three years using an in-situ weather station that collected irradiance, wind speed and direction, temperature, and pressure. Finally, as the entire control system was simulated step by step using MATLAB/Simulink, the components and systems behavior graphs are shown to lead to analysis and conclusion remarks.**

***Keywords*— buck converter; micro-grid; model predictive controller; photovoltaic; wind turbine.**

I. INTRODUCTION

The current methods for energy production are not sustainable, mainly due to environmental reasons and the lack of responsible use of resources [1]. Therefore, the demand for renewable energy, smart electrification, and rational use of electricity are important factors that will provide answers to the global energy challenge. Also, the scheme currently used for the generation of energy is made from fossil fuels, hydroelectric, or nuclear reactors, which are centralized, and the distribution includes losses of up to 69%.

In Colombia, 66% of the territory is not connected to the National Grid. The areas are called Off-Grid Zones (OGZ), and their energy requirements are obtained from traditional fuels such as diesel or biomass, or few Renewable Energy Sources projects (RES), mainly small hydro projects. However, social and economic constraints still cause the lack of available energy or its low-quality services for these regions. On the other hand, the energy sector in Colombia is based on free-market policies since 1994, which have caused that current RES initiatives are without potential size and scope because of the lack of economic incentives and the absence of private stakeholders. Furthermore, the Institute of Planning and Promotion of Energy Solutions for Off-Grid Zones (IPSE, by the Spanish acronym) is in charge of creating such projects. It has a Financial Office (FANZI) which have allocated more than USD 85 million since 2003. It is also a victim of a weak legal framework that has been reformed several times and have directed a lot of efforts and resources to administrative and legal processes [2].

In contrast, renewable energy generation does not pollute, is decentralized, and has innovated with concepts such as "smart grid." Smart grids constitute the framework of future sustainable energy systems, allowing the integration of large amounts of renewable energy, improving reliability, quality of supply, and ensuring safety. Therefore, and due to the significant advantages and developments on renewable energy, it is necessary to analyze how energy should be used in a micro-grid with RES, considering that usually the power is supplied without regard if it comes from the network or renewable supply [3]. In this context, it is vital to perform research and development projects related to emerging technologies in such a manner that they achieve greater electrical energy efficiency and lower emissions. Hence, this work model and simulates a DC grid that can get power from different centralized and renewable sources, optimizing generation, and consumption. Therefore, this paper focuses on the value of energy storage devices when operating in combination with intermittent supply from renewable energy sources. Since forecasts never are perfect, a Model Predictive Control (MPC) strategy is used for keeping the

consequences of forecast uncertainties at acceptable levels, as well as for determining the timing of the operation [4]. Instead of compensating forecast uncertainties with fast-acting backup generators or balancing energy [5]–[10]. Besides, the a priori remaining energy can be resupplied to the primary grid to benefit consumer's common needs.

II. Materials And Method

The proposed micro-grid prototype is shown in Fig. 1, which was designed to provide efficient electric supply to the sports complex in Universidad Militar Nueva Granada (UMNG) at Cajicá Campus. This system has a set of twelve PV Modules of 60W (Bosh c-Si-M60 - M260), a generic wind turbine, a battery bank, and the corresponding converters. The power regulation is performed by the MPC controller designed by the Davinci Research Group.

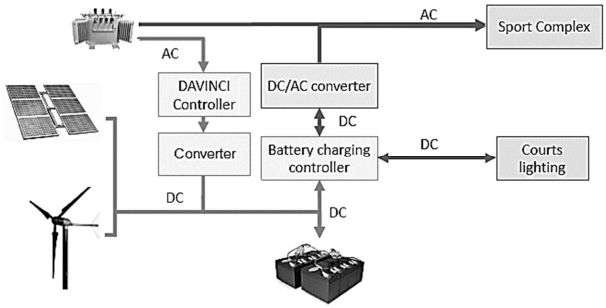

Fig. 1 The system used as a prototype for modeling

The first developed models were the power generators and the storage device, i.e., photovoltaic panels, wind turbines, and batteries. Also, to ensure consistent power to the batteries, it was designed a rectifier with a Buck converter, which is described below.

A. Photovoltaic module model

A photovoltaic (PV) module can be represented as an electrical circuit based on the sunlight-generated current I_{ph} as the source (called photocurrent), with a diode connected in anti-parallel and its current I_d, as well as a parallel resistor R_p with current I_p and a series resistor R_s with the circuit output current I, as proposed by previous studies [11],[12]. The equation that describes the PV model dynamics can be obtained via Kirchhoff's current law, as shown in Eq. 1.

$$I = I_{ph} - I_d - I_p \tag{1}$$

These mathematical approaches have the nonlinearity of the diode and three sets of parameters provided by the manufacturer. Electrochemical constants can be assumed according to climatic and electromechanical conditions. Constants which can be calculated from measures and equations are related to the intrinsic PV physical behavior. Most of the authors use to simplify the mathematical model to reduce the number of unknown parameters via assumptions on the physical cell behavior [11], which are necessary to make the model more accessible and faster to compute. However, parameters based on experimental measures were preserved to assure accuracy and suitability when including real on-site conditions information, similar to the work developed in [13]. This makes it suitable to be used in an integrated energy system, even when it does not take the loss of power into account.

Ohm´s law can define the parallel resistance current, and I_{ph} as a relative value considering the effect of temperature variations in the cells (Eq. 2 and 3).

$$I_p = \frac{V + R_s I}{R_p} \tag{2}$$

$$I_{ph} = \frac{G}{G_{ref}}(I_{ph,ref} + \mu_{sc}\Delta T) \tag{3}$$

where V is the voltage on the diode, G is irradiance, G_{ref} is irradiance at Standard Test Conditions (STC), $I_{ph,ref}$ is the photocurrent at STC, T_c is the temperature of the cell, thus $\Delta T = Tc - T_{c,ref}$ $(T_{c,ref} = 298\,K)$, and μ_{sc} is the temperature coefficient of short circuit current (from manufacturer).

The current I_d is based on the Shockley ideal diode, which sets *I-V* behavior in either forward or reverses setup (Eq. 4).

$$I_d = I_o\left[exp\left(\frac{V + IR_r}{a}\right) - 1\right] a = AN_sV_T \tag{4}$$

A is the ideality factor for monocrystalline silicon cells, N_s is the number of PV cells connected in series and V_T is the thermal factor, defined in Eq. (5) in terms of the Boltzmann constant k, electron charge q, and cell temperature T_c. In Eq. (6) it is defined the reverse saturation or leakage current I_o.

$$V_T = k\frac{T_c}{q} \tag{5}$$

$$I_o = I_{o,ref}\left(\frac{T_c}{T_{c,ref}}\right)^3 exp\left[\left(\frac{q\varepsilon G}{Ak}\right)\left(\frac{1}{T_{c,ref}} - \frac{1}{T_c}\right)\right] \tag{6}$$

The equation shown above depends on electrochemical constants, including the material (silicon) bandgap energy εG, as well as the temperature and the reference leakage current $I_{o,ref}$, defined in Eq. (7) in terms of the voltage at open circuit $(I = 0, V = V_{oc})$ and the short-circuit current $(V = 0, I = I_{sc})$ at STC conditions.

$$I_{o,ref} = I_{sc}exp\left(\frac{-V_{oc,ref}}{a}\right) \tag{7}$$

Finally, device-owned parameters (from manufacturer) were taken from a silicon cell PV module as reference (Bosch c-Si M60-M260). In Table 1, P_{mp}, I_{mp} and V_{mp} are max power, current for max power, and voltage for max power, respectively (tested by manufacturer).

The block diagram of all equations was implemented in Matlab/Simulink and is shown in Fig. 2 (blocks α, I_{o_ref}, I_o, I_{ph}, I and R_p calculate those parameters). However, R_p and R_s need to be obtained. The first by using Eq. 8.

$$R_p = \frac{R_r + I_{mp}R_s}{I_{sc,ref}m - \frac{P_{mp}}{V_{mp}}}; \tag{8}$$

$$m = 1 - exp\left[\frac{V_{mp} + R_s I_{mp} - V_{oc}}{a}\right] + exp\left(\frac{-V_{oc}}{a}\right)$$

TABLE 1
PHOTOVOLTAIC MODULE PARAMETERS

Devised-owned parameters		**Constants at STC**	
Parameter	**Value**	**Parameter**	**Value**
N_s	60	k	$1.381x10^{-23}$
P_{mp}	260	q	$1.602x10^{-19}$
V_{mp}	30.71	G_{ref}	1000
I_{mp}	8.47	$T_{c,ref}$	298
I_{sc}	9.02	Variables to be obtained	
V_{oc}	38.1	R_s	R_p
μ_{sc}	3.1	I_{ph}	I_o
A	1.2	Inputs	
εG	1.12	G	T_c

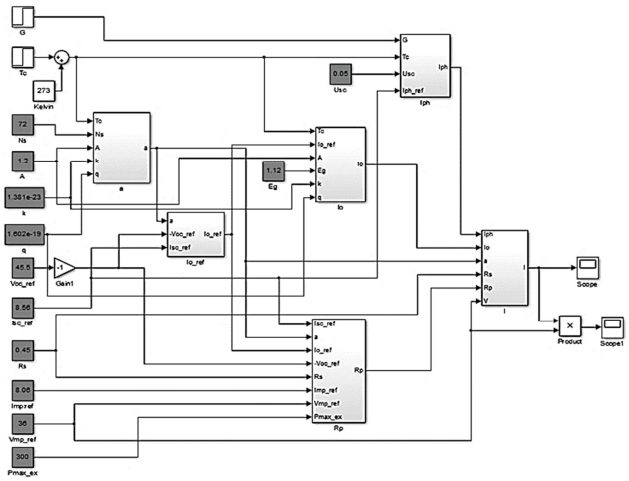

Fig. 2. Simulation of the PV module in Matlab/Simulink

Several values of R_s were proposed to compute the most appropriate value of R_p for reaching the maximum power established by the manufacturer. Fig. 3 shows the current vs. voltage behavior of the presented model at different values of R_s, being $R_s = 0.25\Omega$ the value to reach max current and voltage, named by the manufacturer as I_{mp} and V_{mp} in Table 1.

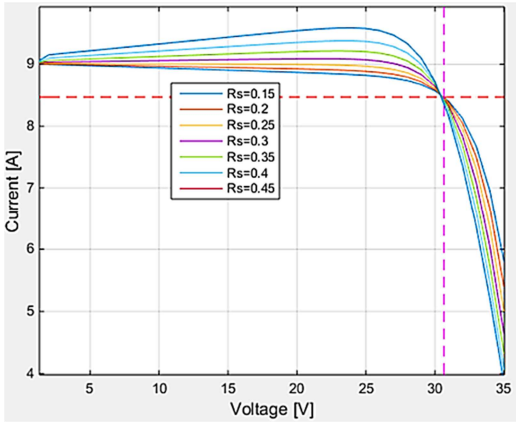

Fig. 3. Photovoltaic module simulation with different values of R_s. Horizontal and vertical dashed lines correspond to I_{mp} and V_{mp}, respectively

Once defined the most suitable values of R_s and R_p, the entire PV model was simulated with the given values of P_{mp}, I_{mp} and V_{mp}. The results are shown in Fig. 4.

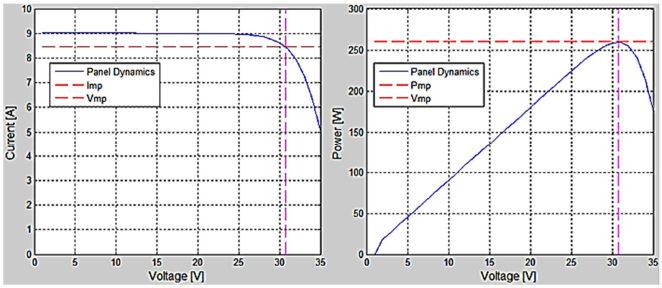

Fig. 4. PV module simulation. Charts of current-voltage and Power-voltage.

B. *Wind Turbine Model*

This section describes the modeling of a wind turbine and the simplified model of the blades. To model a wind turbine, it must be considered a load to which the blades can react in various ways and then have more than twenty degrees of freedom in their reaction. Therefore, it is necessary to obtain its behavior using techniques of modal analysis [14]. These models used to be too complicated for design purposes, so a model simplification must be made to obtain a good representation of the device dynamics, using the main dynamical features and parameters, as shown in Table 2 [15].

TABLE II
WIND TURBINE MODEL PARAMETERS

Parameter	Description	Value
V_w	Wind Speed (m/s)	5
Generator Parameters		
ρ	The specific density of air (Kg/ m^3)	1.23
r_r	The radius of rotor (m)	1
N	Gearbox ratio	4
I_g	Generator inertia (Nms^2)	$2.5x10^{-4}$
J_r	Rotor moment of inertia (Nms^2)	$3x10^{-2}$
R_{rot}	Rotor electric resistance (Ohm)	$9.91x10^{-4}$
B_r	Rotor damping (Nms)	$2.4x10^{-2}$
B_g	Generator damping (Nms)	$5.5x10^{-3}$
K_r	Rotor Hardness (Nm)	$1.5x10^{-4}$
K_g	Generator Hardness (Nm)	$1.5x10^{-4}$
L_i	Rotor electric inductance (H)	$1.526x10^{-3}$
L_g	Armature electric inductance (H)	$8.21x10^{-5}$
A_r	Rotor area (m^2)	3.14
J_{re}	Reflected inertia	$1.9x10^{-3}$
B_{eq}	Equivalent damping	$7x10^{-3}$
K_{eq}	Equivalent Hardness	$1.59x10^{4}$
Dynamic coefficients of the blades		
C_1	Coefficient	$5.176x10^{-1}$
C_2	Coefficient	116
C_3	Coefficient	0.4
C_4	Coefficient	5
C_5	Coefficient	21
C_6	Coefficient	$6.8x10^{-3}$
β	Blade pitch angle	-5

The tip-speed ratio (TSR), denoted as λ, is the ratio between the linear speed of the blade tip and the wind speed [1] and sets the fraction of available power extracted from

the wind by the turbine rotor. In a fixed-speed wind turbine, the blade tip speed is relatively constant since the rotor is connected to the induction generator via a gearbox, and the generator is the one directly connected to the grid. This can be calculated via the rotor radius and angular speed Eq. 9.

$$\lambda = \frac{r_r \omega_r}{V_\omega} \tag{9}$$

The TSR and the user-defined blade pitch angle β, are used to calculate the rotor power coefficient, denoted by C_p [16]. This coefficient is a measure of the rotor efficiency and is calculated via Eq. 10, 11, and 12.

$$C_p = C_1\left(\frac{C_2}{\lambda_i} - C_3\beta - C_4\right)e^{-\frac{C_5}{\lambda_i}} + C_6\lambda \tag{10}$$

$$\frac{1}{\lambda_i} = \frac{1}{\lambda + 0{,}08\beta} - \frac{0{,}035}{\beta^3 + 1} \tag{11}$$

$$C_p = \frac{P_r}{P_\omega} \tag{12}$$

To define the aerodynamic torque, it is necessary to calculate the kinetic energy E Eq. 13, the mass flow $\dot{m}$ Eq. 14, the power of the wind P_w through an area A Eq. 15 and power of rotor P_r Eq. 16, which are given by [17].

$$E = \frac{1}{2}m{V_\omega}^2 \tag{13}$$

$$\dot{m} = \rho A V_\omega \tag{14}$$

$$R_r = \frac{1}{2}\rho A {V_\omega}^3 \tag{15}$$

$$P_r = \frac{1}{2}\rho C_p \pi {r_r}^2 {V_\omega}^3 \tag{16}$$

The aerodynamic torque can be obtained via Eq. 17 or 18.

$$T_r = \frac{P_r}{\omega_r} \tag{17}$$

$$T_r = \frac{\frac{1}{2}\rho C_p \pi {r_r}^2 {V_\omega}^3}{\omega_r} \tag{18}$$

The gear drive system of the wind turbine can be represented by a two-mass model connected by one shaft [1].

The rotational system is described by Eq. 19 and 20, but Eq. 21-23 are used to simplify it. These equations give the equivalence of the low-speed shaft to the high-speed shaft.

$$J_{re}\ddot{\theta}_{re} = -B_{eq}\left(\dot{\theta}_{re} - \dot{\theta}_g\right) - K_{eq}\left(\theta_{re} - \theta_g\right) + \frac{T_{re}}{N} \tag{19}$$

$$J_g\ddot{\theta}_g = -B_{eq}\left(\dot{\theta}_g - \dot{\theta}_{re}\right) - K_{eq}\left(\theta_g - \theta_{re}\right) + T_g \tag{20}$$

$$J_{re} = \frac{J_r}{N^2} \tag{21}$$

$$\omega_{re} = N\omega_r \tag{22}$$

$$T_{re} = \frac{T_r}{N} \tag{23}$$

Finally, the state variables are obtained from the dynamic model, as shown in Eq. 24.

$$\dot{\theta}_{re} = \omega_{re}, \qquad \ddot{\theta}_{re} = \dot{\omega}_{re}, \qquad \dot{\theta}_g = \omega_g, \qquad \ddot{\theta}_g = \dot{\omega}_g \tag{24}$$

Besides, Eq. 25 describes a turbine generator model.

$$L_g\dot{i_g} = L_i\omega_{re} - R_{rot}i_g \tag{25}$$

The dynamic characteristics were not taken into account for the simulation. The system model is represented in matrix form in Eq. 26 and simulated in Matlab/Simulink (Fig. 5 shows the block diagram and Fig. 6 shows the time response).

$$\begin{bmatrix}\dot{\omega}_{re}\\ \dot{\theta}_{re}\\ \dot{i_g}\end{bmatrix} = \begin{bmatrix}-\frac{B_r}{J_r} & 0 & 0\\ 1 & 0 & 0\\ \frac{L_i}{L_g} & 0 & -\frac{R_{rot}}{L_g}\end{bmatrix}\begin{bmatrix}\omega_{re}\\ \theta_{re}\\ i_g\end{bmatrix} + \begin{bmatrix}\frac{1}{T_r}\\ 0\\ 0\end{bmatrix}[T_r]$$

$$y = [0 \quad 0 \quad 1]\begin{bmatrix}\omega_{re}\\ \theta_{re}\\ i_g\end{bmatrix} \tag{26}$$

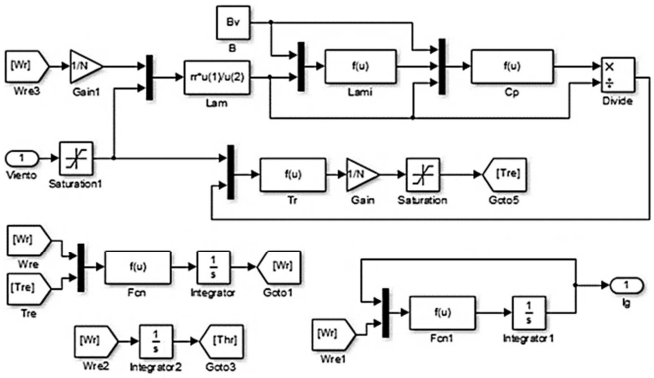

Fig. 5. Wind turbine model in Matlab/Simulink.

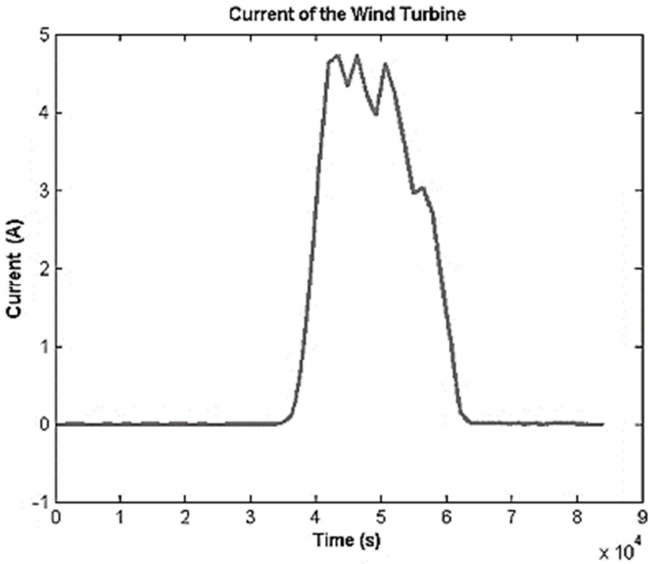

Fig. 6. Time Response of the wind turbine model in Matlab/Simulink.

C. Battery Model

The Battery block implements a generic dynamic model parameterized to represent the most popular types of rechargeable batteries. The parameters of the equivalent circuit can be modified to represent a particular battery type, based on its discharge characteristics. The model can be expressed by the open-circuit voltage (OCV) or electromotive force (EMF) E_0, the voltage in the battery terminals V_t, internal resistance R_i, discharge current I and

state of charge (SOC) Q. This model describes the battery electrochemical behavior and is described in Eq. 27, 28, and 29 (parameters in Table 3).

$$E = E_0 - K\frac{Q}{Q - \int idt} + Ae^{-B\int idt} \quad (27)$$

$$V_t = E - R_i i \quad (28)$$

$$E_{Batt} = E_0 - K\frac{Q}{Q - i_t} i_t - Ri - K\frac{Q}{Q - it} i^* + Ae^{-Bit} \quad (29)$$

TABLE III
BATTERY MODEL PARAMETERS

Param.	Description	Value
E_{Batt}	Battery voltage (V)	
E_0	Nominal battery voltage or open circuit (V)	48
K	Polarization voltage constant (Ah^{-1}) or polarization resistance (ohms)	
i^*	Filtered current (A)	
i	Battery current (A)	
i_t	Current battery charge (Ah)	
Q	Maximum battery capacity (Ah)	140
A	Exponential zone amplitude (V)	0.45
B	Exponential zone time constant inverse capacity $(Ah)^{-1}$	1.11
R	Internal resistance (ohms)	$3.692x10^{-2}$
$Exp(t)$	Exponential zone dynamics (V)	
$u(t)$	Battery mode: 0 in discharge and 1 in charge	

Where the exponential term of Eq. 29 is determined by the type of battery, here Li-Ion, which is simulated and selected in the block configuration in Simulink®. This term describes the non-linear phenomenon of charge and discharge modes, expressed by Eq. 30, where $exp(t)$ is the exponential zone voltages, $i(t)$ is battery current, and $u(t)$ is the charging mode (charge/discharge) [14],[18].

$$exp(t) = B\,|i(t)|(-exp(t) + Au(t)) \quad (30)$$

Eq. 31 and 32 show the battery voltage at a charge ($i^* > 0$) and the discharge mode ($i^* < 0$), respectively.

$$E_{Batt} = E_0 - K\frac{Q}{Q - i_t} i_t - Ri - K\frac{Q}{Q - i_t} i^* + Exp(t) \quad (31)$$

$$E_{Batt} = E_0 - K\frac{Q}{Q - i_t} i_t - Ri - K\frac{Q}{|i(t)| - 0{,}1Q} i^* + exp(t) \quad (32)$$

To solve the slow dynamic behavior in the response of voltage and current flow, the filtered current i^* is used in the algebraic loop, generated in the Simulink simulations [19]. A typical discharge curve is shown in Fig. 7 and exposes the nonlinear behavior of the battery voltage [18] - [20].

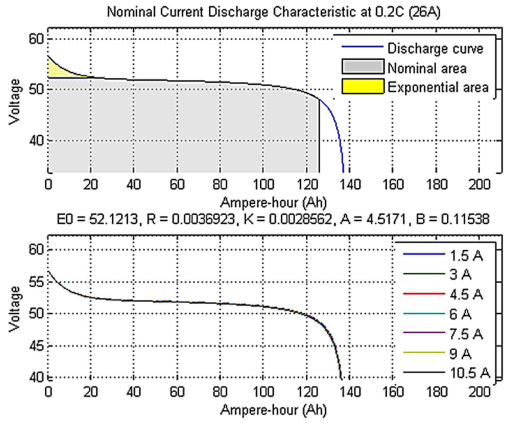

Fig. 7. Battery discharge curve.

D. Buck Converter Model:

The typology of a conventional Buck converter is a parallel RLC circuit, which a power switch S, inductor L, capacitor C and resistance R representing the load on the battery circuit, simulated as a time-varying sine-wave. The dynamic process of the circuit can be described by ordinary differential Eq. 33 and 34.

$$L\frac{di}{dt} it = -v + Eu \quad (33)$$

$$C\frac{dv}{dt} = i + Rv \quad (34)$$

The state variables are $x_1 = i$, $x_2 = v$ and therefore the state space equations are Eq. 35 and 36 [21], [22].

$$\dot{x}_1 = -\frac{1}{L}x_2 + \frac{E}{L}u \quad (35)$$

$$\dot{x}_2 = -\frac{1}{C}x_1 + \frac{R}{C}x_2 \quad (36)$$

To ensure the DC bus voltage of the batteries, a controller is implemented in state-space representation. See Fig. 8 [23].

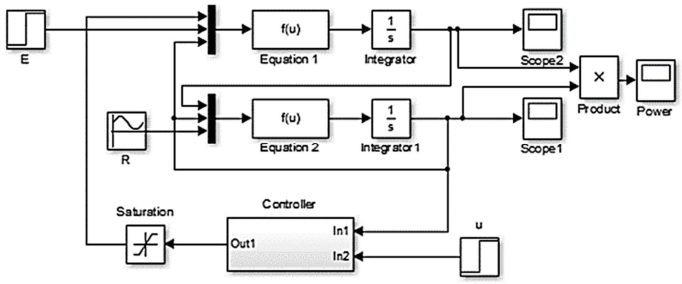

Fig. 8 Block diagram of the system in state-space with a controller

This controller must be reactively robust, responding to disturbances produced by the load resistance to reach a reference current. Hence, a digital servo-controller with state feedback was designed. It was necessary to determine the integral gain constant k_1 and feedback gain matrix of k_2 to obtain a response with dead oscillations, all shown in Fig. 9.

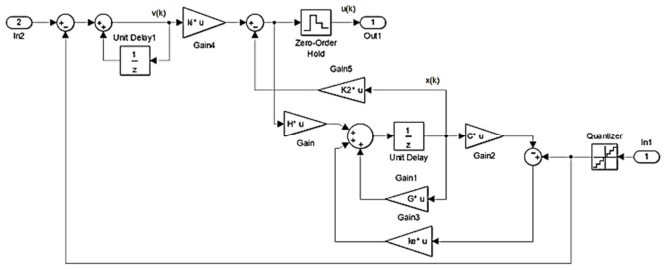

Fig. 9. Block diagram of the digital control

The discrete servo-system constants were calculated by the Ackerman method using packed storage matrices and two design parameters: damping ratio $\xi = 0.7$, response time $t = 10\,\mathrm{s}$. It is important to clarify that the system representation was not done with the conventional state-space blocks included in Matlab because they do not allow to include the lag resistance R as a time-variable signal to the state matrix A.

The output signal can be obtained from the resistance sine wave, in terms of voltage and current (Fig. 10). The system responds according to charge variations, varying the supply current, and maintaining the voltage level required.

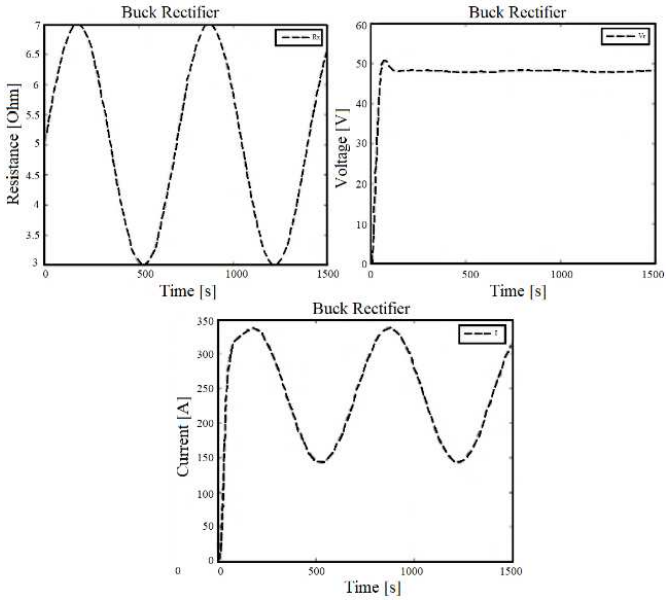

Fig. 10. Buck converter response with the controller.

E. System Simulation with Model Predictive Controller

The purpose of this work is to ensure the proper batteries and continuous energy supply to the lighting system. Thus, a Model Predictive Controller – MPC was implemented. This control system defines the state of charge (SOC) as the controlled variable, while the reference is the DC bus voltage, and the manipulated variable is the rectifier (see Fig. 11).

An MPC is capable of determining which renewable energy source charges the batteries according to the value of supply, i.e., during periods of high solar irradiance, the batteries charging depends on the PV modules' power.

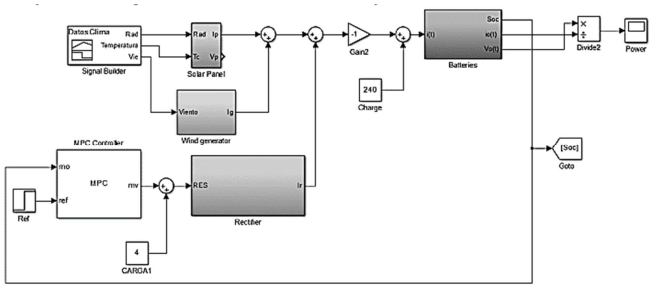

Fig. 11. Renewable energy system with Model Predictive Controller

In contrast, in high wind speed, it depends on the wind turbine, and in the absence of power supply from renewable resources, the charging process depends on the rectified local grid. Fig. 12 shows data of a daily solar irradiance and wind speed during a random day.

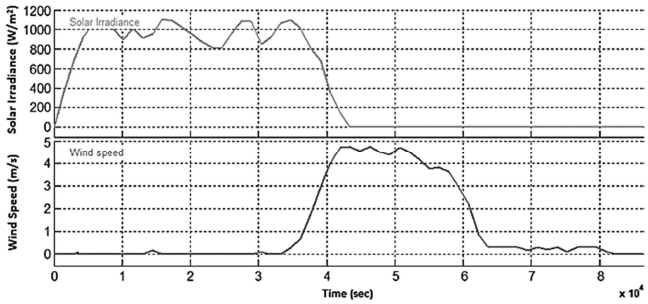

Fig. 12. Weather data collected in UMNG Campus

The main advantage of using MPC is the fact that it allows the current time slot to be optimized while keeping future ones into account [6], [8]–[10]. This is achieved by optimizing a finite time-horizon, but only implementing the current time slot. Only the first step of the control strategy is implemented, then the plant state is sampled again, and the calculations are repeated starting from the new current state, yielding a new control and a new predicted state path. Prediction horizon keeps being shifted forward, and thus it is also called receding horizon control [5]. The optimization cost function is given by Eq. 37, considering design boundaries (lower/upper).

$$\begin{bmatrix}\dot{x}_1\\ \dot{x}_2\end{bmatrix} = \begin{bmatrix}0 & -\frac{1}{L}\\ \frac{1}{C} & -\frac{R}{C}\end{bmatrix}\begin{bmatrix}x_1\\ x_2\end{bmatrix} + \begin{bmatrix}\frac{E}{L}\\ 0\end{bmatrix}[u]$$
$$y = [0 \quad 1]\begin{bmatrix}x_1\\ x_2\end{bmatrix} \tag{37}$$

With $x_i = i - th$ as the controlled variable (batteries SOC), $r_i = i - th$ as the reference variable (required voltage of the bus), $u_i = i - th$ as the manipulated variable (rectifier current), ω_{xi} as the weighting coefficient reflecting the relative importance of x_i, ω_{ui} as the weighting coefficient penalizing relative big changes in u_i.

III. Results And Discussion

Fig. 13 shows how the MPC responds to load variations caused by energy demands by ensuring the DC bus voltage.

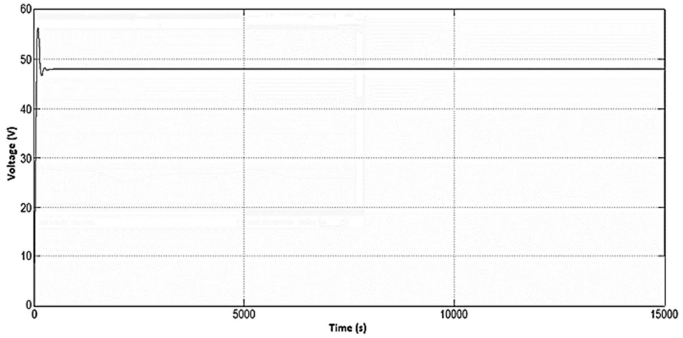

Fig. 13 The voltage of the DC bus

These variations in energy produce changes in the battery SOC (Fig. 14). A quick charging process can be seen at the beginning of the chart, followed by several compensations to maintain the reference of 80% of SOC.

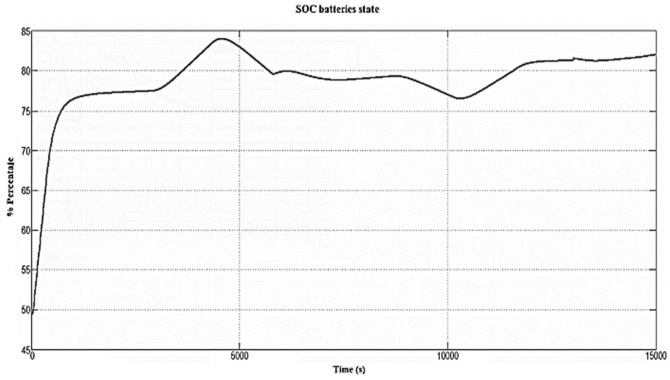

Fig. 14. Batteries State of Charge

Despite these changes, the control signal compensates for the impedance maintaining a level of 4Ω (Fig. 15).

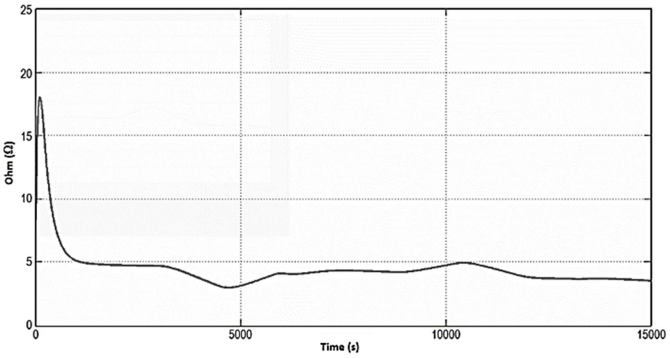

Fig. 15 The control signal generated by the MPC

This compensation is made from the control signal and employing a current rectifier (Fig. 16). In the graph, the current reaches a max value of 500 A (saturated), to emulate the protection system and behavior of the Powerex® R620 General Purpose Rectifier (500 A). This also causes the dynamic response of the system to present delays. Fig. 17 shows the PWM signal of the DC converter.

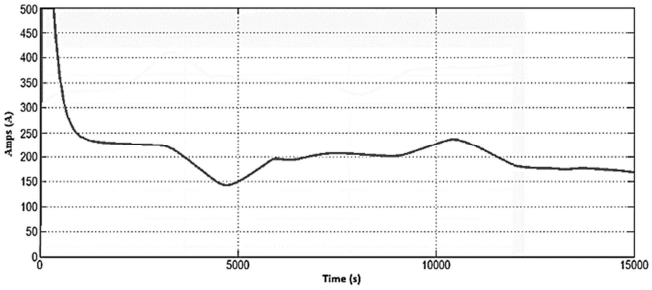

Fig. 16. Rectifier current

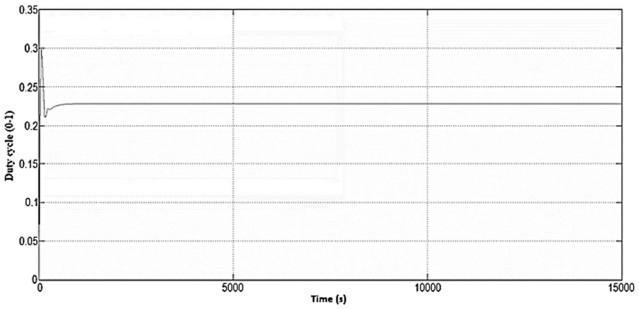

Fig. 17. PWM signal of the DC converter.

IV. Conclusion

A nonlinear equation of current approximates the abstraction of the photovoltaic module in terms of two weather variables (irradiance and temperature) and the desired output voltage. The non-linearity is mainly given by the exponential dynamics of the antiparallel diode. Therefore, the $I-V$ chart shows a decreasing curve that begins when short-circuit ($V=0, I=I_{sc}$) and at open circuit ($I=0, V=V_{oc}$). Also, although the PV module works with a nominal voltage of $V=24$V, the maximum power point occurs when $V=V_{mp}=30.71\,\text{V}$, which implies $I=I_{mp}=9.02\,\text{A}$ and thus $P=P_{mp}=260\,\text{W}$ just as tested by the manufacturer.

The environmental resources at the installation site of power microgrid were measured by a weather station and used as input parameters of the simulation, which concluded that there is not a significant contribution from wind power (low average wind speed). Thus the wind turbine model was sized as a small DC power generator. Therefore, the only feasible and fully available power resource will be generated by photovoltaic panels, making it the primary source. Nevertheless, the energy produced by the wind turbine is not underestimated, in fact, it is included as a disturbance to the energy generated on the grid, so still contributing to the total generation. This means that this DC microgrid also includes several low production energy sources to charge the batteries, adding them as disturbances to the control system for energy production and thus increase the energy supplied to the load.

Besides, as the main result of this work, it was realized that the implemented Model Predictive Controller could significantly reduce the energy consumption in conventional and non-renewable energy sources, such as those based on Diesel fuel, which is a major power source in stand-alone grids in non-interconnected zones. This considering that diesel turbines still are needed to be used as the rectified power sources for the Buck converter of the proposed grid. Still, it can be enhanced by harnessing the weather forecasting and the predictive controller itself to pre-heat the

turbine and thus increasing efficiency, i.e., turning the reactive controller of a regular diesel turbine into a predictive controlled one.

ACKNOWLEDGMENT

The Vice Rector for Research of Universidad Militar Nueva Granada financially supported this work, through the project ING-1577 titled "Development, automation, and control of a hybrid renewable resources plant."

REFERENCES

[1] J.F. Manwell, J.G. McGowan and A.L. Rogers. Wind Energy Explained: Theory, Design and Application, Second edition. Wiley John + Sons. 2010

[2] B. Ruíz and V. Rodríguez-Padilla. Renewable energy sources in the Colombian energy policy, analysis and perspectives. Energy Policy, 34(18), 3684-3690. 2006

[3] C. Chuanchuan, Z. Jun and J. Panpan. Multi-agent system applied to energy management system for renewable energy micro-grid. 5th IEEE International Conference on Power Electronics Systems and Applications PESA. December 2013.

[4] F. Chen, L.V. Snyder and S. Kishore. Efficient algorithms and policies for demand response scheduling. Journal of Energy Engineering, 141(1). 2015.

[5] M. Arnold and G. Anderson. Model predictive control of energy storage including uncertain forecasts. 17th Power Systems Computation Conference PSCC. August 2011.

[6] C. Bordons, F. García-Torres and L. Valverde. Optimal energy management for renewable energy microgrids. Revista Iberoamericana de Automática e Informática Industrial RIAI. 12(2), 117-132. 2015.

[7] F. García and C. Bordons. Regulation service for the short-term management of renewable energy microgrids with hybrid storage using model predictive control. 39th Annual Conference of the IEEE Industrial Society IECON. November, 2013.

[8] J. Rawlings and K. Muske. The stability of constrained receding horizon control. IEEE Transactions on Automatic Control. 38(10), 1512-1516. 1993.

[9] M.S. Tsoeu and T. Koetje. Unconstrained MPC tuning for prediction accuracy in networked control systems. IEEE International Conference on Networking, Sensing and Control. 2011.

[10] L. Valverde, C. Bordons and F. Rosa. Power management using model predictive control in a hydrogen-based microgrid. 38th Annual Conference on IEEE Industrial Electronics Society IECON. October, 2012.

[11] H. Bellia, R. Youcef and M. Fatima. A detailed modelling of photovoltaic module using MATLAB. Journal of Astronomy and Geophysics. 3(1), 53-61. 2014.

[12] K. Ishaque, Z. Salam, H. Taheri and Syafaruddin. Modeling and simulation of photovoltaic (PV) system during partial shading based on a two-diode model. Simulation Modelling Practice and Theory. 19(7), 1613-1626. 2011.

[13] M. Mauledoux, O. Avilés, E. Mejía-Ruda and O.I. Caldas. Analysis of autoregressive predictive models and artificial neural networks for irradiance estimation. Indian Journal of Science and Technology. 9(38), 1-7. 2016.

[14] S. Georg, H. Schulte and H. Aschemann. Control-oriented modelling of wind turbines using a takagi-sugeno model structure. IEEE International Conference on Fuzzy Systems. June, 2012.

[15] A. Abo-Khalil and D.C. Lee. Dynamic modelling and control of wind turbines for grid-connected wind generation system. 37th IEEE Power Electronics Specialists Conference. 2006.

[16] C.Y. Tang, Y. Guo and J.N. Jiang. Nonlinear dual-mode control of variable-speed wind turbines with doubly fed induction generators. IEEE Transactions on Control Systems Technology. 19(4), 744-756. 2011.

[17] M.S. Alam and D.W. Gao. Modelling and analysis of a wind/PV/fuel cell hybrid power system in HOMER. 2nd IEEE Conference on Industrial Electronics and Applications. Mayo, 2007.

[18] O. Tremblay and T. Koetje. Unconstrained MPC tuning for prediction accuracy in networked control systems. IEEE International Conference on Networking, Sensing and Control. April, 2011.

[19] A. Almendros. Regulación eólica con baterías en vehículos eléctricos. MasterThesis. Universidad de Sevilla, España. 2012

[20] K. Bae, S. Choi, Y. Wong and C. Jung. LiFePO4 dynamic battery modelling for battery simulator. IEEE International Conference on Industrial Technology (ICIT). February, 2014

[21] A. Bragado. Análisis y diseño de un rectificador trifásico elevador PWM. MasterThesis Universidad Carlos III de Madrid. July 2010.

[22] L. Hernández-Fonseca, D. Gómez-León and O. Hernández-Gómez. Rectificador monofásico con corrección del factor de potencia usando un convertidor boost. Tecnura. 16(33), 23-34. 2012

J. Pérez, C, Núñez and V. Cárdenas. Control lineal para un rectificador monofásico PWM Puente completo. RIEE&C. 7(2), 8-15. 2009.